CHAPTER 11

CAPILLARY BRIDGES AND CAPILLARY-BRIDGE FORCES

The importance of capillary bridges has been recognized for many systems and phenomena like consolidation of granules and soils, wetting of powders, capillary condensation and bridging in the atomic-force-microscope measurements, etc. The capillary bridge force is oriented normally to the plane of the three-phase contact line and consists of contributions from the capillary pressure and surface tension. The toroid (circle) approximation can be applied to quantify the shape of capillary bridges and the capillary-bridge force. More reliable results can be obtained using the exact profile of the capillary bridge, which is determined by the Plateau sequence of shapes: (1) nodoid with "neck", (2) catenoid, (3) unduloid with "neck", (4) cylinder, (5) unduloid with "haunch", (6) sphere and (7) nodoid with "haunch". For the shapes (1-5) the capillary-bridge force is attractive, it is zero for sphere (6) and repulsive for the nodoid (7). Equations connecting the radius of the neck/haunch with the contact angle and radius are derived. The procedures for shape calculations are outlined for the cases of bridges between a plane and an axisymmetric body, and between two parallel planes. In the asymptotic case, in which the contact angle belongs to the range $70° < \varphi_c < 90°$, the elliptic integrals reduce to elementary algebraic functions and the capillary bridge can be described in terms of the toroid approximation. Some upper geometrical and physical stability limits for the length of the capillary bridges are considered; the latter can be established by analysis of diagrams of volume vs. pressure. Attention is paid also to the thermodynamics of nucleation of capillary bridges between two solid surfaces. Two plane-parallel plates are considered as an example. The treatment is similar for *liquid-in-gas* bridges between two hydrophilic plates and for *gas-in-liquid* bridges between two hydrophobic plates. Nucleation of capillary bridges is possible when the distance between the plates is smaller than a certain limiting value. Equations for calculating the work of nucleation and the size of the critical (and/or equilibrium) nucleus are presented.

11.1. ROLE OF THE CAPILLARY BRIDGES IN VARIOUS PROCESSES AND PHENOMENA

McFarlane and Tabor [1] studied experimentally the adhesion of spherical beads to a flat plate. They established that in clean dry air the adhesion was negligible. In humid atmosphere, however, marked adhesion was observed, particularly with hydrophilic glass surfaces. At saturated humidity the adhesion was the same as that observed if a small drop of water was placed between the surfaces [1], see Fig. 11.1. Similar results were obtained in the earlier experimental studies by Budgett [2] and Stone [3]. The formation of a liquid bridge between two solid surfaces can lead to the appearance of attractive (adhesive) force between them owing to the decreased pressure inside the liquid bridge and the direct action of the surface tension force exerted around the annulus of the meniscus. We should say from the very beginning that in some cases the force due to capillary bridge can be also repulsive, see Eq. (11.15) below. In all cases this force is perpendicular to the planes of the three-phase contact lines (circumferences) on the solid surfaces, in contrast with the lateral capillary forces considered in Chapters 7-10.

The importance of the capillary bridges has been recognized in many experimental and practical systems [4]. For example, the effect of capillary bridges is essential for the assessment of the water saturation in soils and the adhesive forces in any moist unconsolidated porous media [5-7]; for the dispersion of pigments and wetting of powders [8]; for the adhesion of dust and powder to surfaces [9]; for flocculation of particles in three-phase slurries [10]; for liquid-phase sintering of fine metal and polymer particles [11,12]; for obtaining of films from latex and silica particles [13-15]; for calculation of the capillary evaporation and condensation in various porous media [16-19]; for estimation of the retention of water in hydrocarbon reservoirs [20], and for granule consolidation [21,22]. The action of capillary-bridge force is often detected in the experiments with atomic force microscopy [23-25]. The capillary-bridge force is also one of the major candidates for explanation of the attractive hydrophobic surface force [26-31], see Section 5.2.3 above.

Pioneering studies (both experimental and theoretical) of capillary bridges have been undertaken by Plateau, who classified the shapes of the capillary bridges (the surfaces of
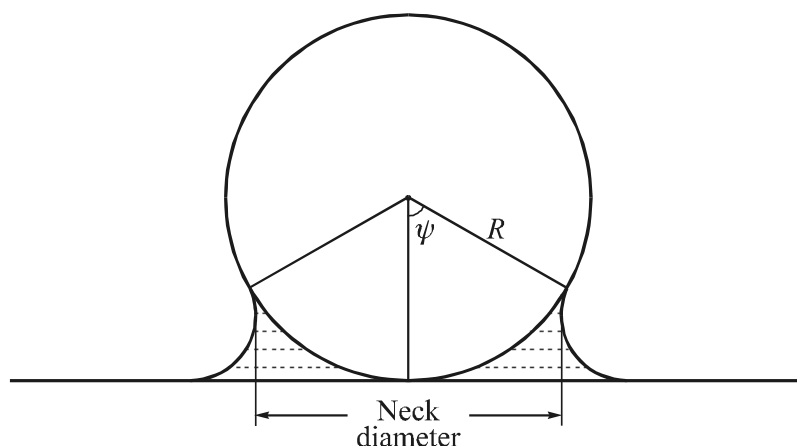
Fig. 11.1. Liquid bridge between a spherical particle and a planar solid surface.

constant mean curvature) and investigated their stability [32-34]. The study of the instability of cylindrical fluid interfaces by Plateau was further extended by Rayleigh, who considered also jets of viscous fluid [35-38]. The shapes of capillary bridges between two solid spheres and between sphere and plate were experimentally investigated by McFarlane and Tabor [1], Cross and Picknett [39], Mason et al. [40-41], Erle et al. [42]. Exact solutions of the Laplace equation of capillarity for the respective bridges have been obtained in the works by Fisher [7], Melrose [43], Erle [42], Orr et al. [4]. In some cases appropriate simpler approximate solutions can be applied [4, 41, 44-46]. All these studies deal with capillary bridges between *two solids*.

Capillary bridges can appear also between *solid* and *fluid* phases. Taylor and Michael [47] studied (both theoretically and experimentally) the formation and stability of holes in a sheet of liquid, see Fig. 2.5. Forcada et al. [48] examined theoretically the appearance of a capillary bridge, which "jumps" from a liquid film to wet the tip of the atomic force microscope. Debregeas and Brochard-Wyart [49] investigated experimentally the nucleation and growth of liquid bridges between a horizontal liquid interface and a horizontal solid plate at a short distance apart. The interaction between solid particle and gas bubble, studied by Ducker et al. [28] and Fielden et al. [50], also leads to the formation of a capillary-bridge-type meniscus.

Capillary bridges between *two fluid* phases are found to have crucial importance for the process of antifoaming by dispersed oil drops by Ross [51], Garrett [52, 53], Aveyard et al. [54-56], and Denkov et al. [57, 58]. When an oil droplet bridges between the surfaces of an aqueous film,

two scenarios of film destruction are proposed: (i) dewetting of the drop would create film rupture [52]; (ii) the oil bridge could have a unstable configuration and film rupturing could happen at the center of the expanding destabilized bridge [53]. The latter mechanism has been recorded experimentally with the help of a high-speed video camera [57] and the results have been interpreted in terms of the theory of capillary-bridge stability [58]. More about the bridging between two fluid phases and the antifoaming action can be found in Chapter 14 below.

Many works have been devoted to the problem of capillary-bridge *stability*; we give a brief review in Section 11.3.4 below. Comprehensive review articles about the progress in this field have been published by Michael [59] and Lowry and Steen [60].

Everywhere in this chapter we consider relatively small bridges and neglect the gravitational deformation of the meniscus.

11.2. DEFINITION AND MAGNITUDE OF THE CAPILLARY-BRIDGE FORCE

11.2.1. DEFINITION

Let us consider an axisymmetric fluid capillary bridge formed between two solid bodies, say two parallel plates, or particle and plate (Fig. 11.1), or two particles (Fig. 11.2), or two circular rings [47]. The presence of capillary bridge will lead to interaction between the two bodies, which can be attractive or repulsive depending on the shape of the bridge (see below). As in the case of lateral capillary forces (see Chapters 7 and 8) the total capillary force F_c is a sum of contributions from the surface tension σ and the meniscus capillary pressure, P_c:

$$F_c = F^{(\sigma)} + F^{(p)} \tag{11.1}$$

Due to the axial symmetry F_c is directed along the z-axis (Fig. 11.2). To calculate the force exerted on the upper particle (Fig. 11.2) one can apply the classical Stevin approach: the upper part of the capillary bridge (above the plane $z = 0$) can be considered to be "frozen" and the z-components of the forces exerted on the system "frozen bridge + upper particle" to be calculated. Thus one obtains $F^{(\sigma)} = -2\pi r_0 \sigma$ and $F^{(p)} = \pi r_0^2 P_c$, and consequently,

$$F_c = -\pi(2r_0\sigma - r_0^2 P_c), \qquad\qquad P_c \equiv P_1 - P_2 \tag{11.2}$$
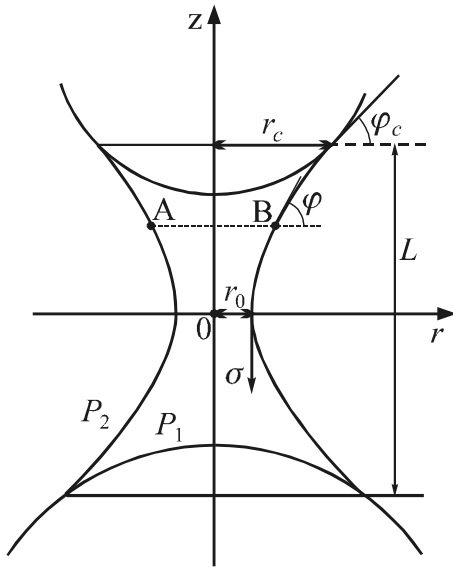
Fig. 11.2. Sketch of the capillary bridge between two axisymmetric particles or bodies. P_1 and P_2 are the pressures inside and outside the bridge of length L; r_0 and r_c are the radii of the neck and the contact line; φ_c and φ are the values of the meniscus slope angle at the contact line and at an arbitrarily chosen section AB.

In Eq. (11.2) negative F_c corresponds to attraction between the two bodies, whereas positive F_c corresponds to repulsion. In spite of the fact that Eq. (11.2) has been obtained for the section across the neck (or the "haunch", see Fig. 2.6b) of the bridge, the total capillary force F_c is independent of the choice of the cross-section. To prove that one first represents the Laplace equation, Eq. (2.24), in the form

$$\sigma\, d(r\sin\varphi)/dr = P_c r \qquad\qquad\qquad \tan\varphi \equiv dz/dr \qquad\qquad (11.3)$$

and then integrates:

$$\sigma(r\sin\varphi - r_0) = \tfrac{1}{2} P_c(r^2 - r_0^2) \qquad\qquad\qquad\qquad\qquad (11.4)$$

Comparing Eqs. (11.2) and (11.4) one obtains the expression for the capillary force F_c corresponding to an arbitrary section of the bridge, say the section *AB* in Fig. 11.2:

$$F_c = -\pi(2r\sigma\sin\varphi - r^2 P_c) \qquad\qquad (0 \le \varphi \le \pi) \qquad\qquad (11.5)$$

Note that Eq. (11.5) can be directly obtained by making the force balance for the section *AB*, in the same way as we did for the section $z = 0$ (Fig. 11.2). Equation (11.4) guarantees that the result for F_c will be the same, irrespective of the choice of the cross-section. If r is chosen to be the radius r_c of the contact line at the particle surface, then $\varphi = \varphi_c$ is the meniscus slope angle at the contact line:

$$F_c = -\pi(2r_c\sigma\sin\varphi_c - r_c^2 P_c) \qquad\qquad (11.5a)$$

Note that the surface tension term in Eq. (11.5) always leads to attraction between the two particles, whereas the capillary pressure term corresponds to repulsion for $P_c > 0$, and to attraction for $P_c < 0$ (in the latter case the bridge is nodoid-shaped with a neck, see Section 11.3.1 for details.

In accordance with the Laplace equation, Eq. (2.19), the capillary pressure $P_c = P_1 - P_2$ of an axisymmetric meniscus can be expressed as follows:

$$P_c = \sigma(1/r_m + 1/r_a), \qquad\qquad (11.6)$$

where r_m and r_a are, respectively, the meridional and azimuthal radii of curvature. In general, r_m and r_a vary from point to point and can have positive or negative sign. The *sign convention* followed in this chapter corresponds to positive r_m and r_a for a sphere. When the capillary bridge has small length L, but relatively large volume, then $r_a \gg r_m$ and Eq. (11.6) can be written in the form

$$P_c \approx \sigma/r_m \qquad\qquad (r_a \gg r_m) \qquad\qquad (11.7)$$

Since P_c = constant (the gravity deformation negligible), then Eq. (11.7) gives r_m = constant, that is the generatrix of the meniscus is a circle in this asymptotic case.

11.2.2. CAPILLARY BRIDGE IN TOROID (CIRCLE) APPROXIMATION

As shown in Chapter 2, in the case of capillary bridges the generatrix of the meniscus is usually an arc of nodoid or unduloid, which are mathematically expressed in terms of elliptic integrals, see Fig. 2.7 and Eqs. (2.50)–(2.52). In some special cases the meniscus can be catenoid, cylinder or sphere, see Section 11.3.1. For the sake of estimates, in the literature the generatrix is often approximated with an arc of *circle*, and correspondingly, the meniscus is described as a part of a *toroid* [1, 4, 39, 41]. In the asymptotic case described by Eq. (11.7) this is the exact profile. When the toroid approximation is used, the meridional radius r_m is uniquely determined by the boundary condition for fixed contact angle at the line of three-phase contact (the Young equation), see e.g. Eq. (11.10) below. On the other hand, in various works the toroid approximation is used with different definitions of the azimuthal curvature radius r_a :
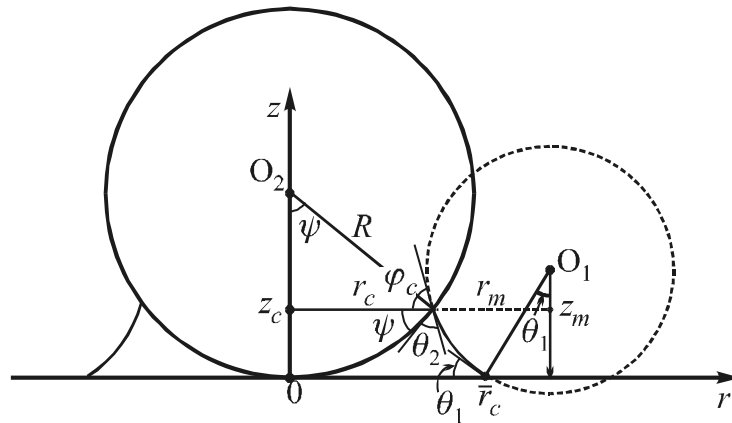
Fig. 11.3. In toroid approximation the generatrix of the profile of the capillary bridge is approximated with a circle (with center at O_2 in the figure). θ_1 and θ_2 are the three-phase contact angles at the surfaces of the solid plate and the spherical particle of radius R, respectively.

$$r_a = r_c/\sin\varphi_c \qquad \text{(maximum possible value of } r_a\text{)} \qquad (11.8a)$$

$$r_a = r_c \qquad \text{(an intermediate value of } r_a\text{)} \qquad (11.8b)$$

$$r_a = r_0 = r_c - r_m(1 - \sin\varphi_c) \qquad \text{(minimum possible value of } r_a\text{)} \qquad (11.8c)$$

where, as before, r_0 is the radius of the "neck" and φ_c is the meniscus slope angle at the contact line, which is a circumference of radius r_c. Actually, for a given capillary bridge, r_a varies from $r_c/\sin\varphi_c$ at the contact line down to r_0 at the "neck". Equation (11.8a) was used by Orr et al. [4] to derive approximate expression for the capillary-bridge force between a spherical particle and a planar plate for arbitrary values of the contact angles. Equation (11.8c) was utilized by Clark et al. [41] for a similar system in the special case of zero contact angle (hydrophilic particle and plate). Below we demonstrate that for $70° < \varphi_c < 90°$ Eq. (11.8b) compares well with the result for the capillary pressure P_c of a symmetric nodoid-shaped bridge with "neck", see Eq. (11.54).

Let us consider the application of the toroid (circle) approximation to the capillary bridge between a spherical particle of radius R and a planar plate, for arbitrary values of the contact angles, denoted by θ_1 and θ_2, see Fig. 11.3. The contact radius and meniscus slope at the *particle* contact line are denoted by r_c and φ_c, respectively; z_c is the distance between the plane of the particle contact line and the planar solid surface. For each of the two circumferences in Fig. 11.3 one can obtain an expression for z_c:

$$R(1 - \cos\psi) = z_c = z_m - r_m \cos\varphi_c , \qquad\qquad z_m = r_m \cos\theta_1 \qquad (11.9)$$

From Eq. (11.9) one can determine the meridional radius of curvature [4]:

$$r_m = -R(1 - \cos\psi)(\cos\theta_1 - \cos\varphi_c)^{-1} \qquad \text{(toroid approximation)} \qquad (11.10)$$

In addition, we notice that $\varphi_c = \pi - (\psi + \theta_2)$ and $r_c = R\sin\psi$, see Fig. 11.3. Then substituting Eqs. (11.6), (11.8a) and (11.10) into Eq. (11.5a) one determines the capillary-bridge force in toroid approximation:

$$F_c = -\pi R\sigma \{\sin(\psi + \theta_2)\sin\psi + (1 + \cos\psi)[\cos\theta_1 + \cos(\psi + \theta_2)]\} \qquad (11.11a)$$

In the same way, but using Eq. (11.8b), instead of Eq. (11.8a), one derives an alternative expression:

$$F_c = -\pi R\sigma \{[2\sin(\psi + \theta_2) - 1]\sin\psi + (1 + \cos\psi)[\cos\theta_1 + \cos(\psi + \theta_2)]\} \qquad (11.11b)$$

A third version of the expression for F_c can be obtained combining Eq. (11.8c) with Eqs. (11.2), (11.6) and (11.10):

$$F_c = -\pi\sigma \frac{1 + \cos\psi}{a\sin\psi} [a\sin\psi - (1 - \cos\psi)(1 - \sin\psi)](a + 1 - \cos\psi) \qquad (11.11c)$$

where $a \equiv \cos\theta_1 + \cos(\psi + \theta_2)$. In spite of the different form of Eqs. (11.11a)–(11.11c) all of them give the same asymptotics for $\psi \to 0$,

$$F_c \approx -2\pi\sigma R(\cos\theta_1 + \cos\theta_2) = 4\pi\sigma R\cos\frac{\theta_1 + \theta_2}{2}\cos\frac{\theta_1 - \theta_2}{2} \qquad (\psi \ll 1) \qquad (11.12)$$

which corresponds to the limiting case of a very small (thin and flat) bridge in the form of ring around the touching point of the sphere and plane [4]. Such a "pendular ring" can be formed between a hydrophilic sphere and a plane owing to a local condensation of water, which gives rise to a strong *adhesion* [1, 61]. However, if the wetting is sufficiently imperfect that $\theta_1 + \theta_2 > \pi$, then F_c has positive sign and corresponds to *repulsion*. For $\theta_1 = \pi/2$ Eq. (11.12) reduces to a formula reported by Cross and Picknett [39]. In the special case of hydrophilic surfaces, $\theta_1 = \theta_2 = 0$, Eq. (11.11c) yields the formula derived by Haynes, see Ref. [41]:

$$F_c \approx -2\pi\sigma R(2\sin\psi + \cos\psi - 1)/\sin\psi \qquad (11.13)$$

For two equal non-zero contact angles, $\theta_1 = \theta_2 = \theta$, Eq. (11.12) reduces to the formula of McFarlane & Tabor [1] $F_c \approx -4\pi\sigma R\cos\theta$. If both the sphere and plane are hydrophilic ($\theta = 0$), then $F_c \approx -4\pi R\sigma$. It is really astonishing that a tiny microscopic pendular ring, localized in the narrow contact zone sphere-plane, can create a force equal to twice the surface tension, 2σ, multiplied by the equatorial length of the sphere, $2\pi R$. However, this force is not due to the direct contribution of the surface tension, $F^{(\sigma)} = -2\pi r_c \sigma \sin\varphi_c$. For $\psi \to 0$ the thickness of the gap $h = R(1 - \cos\psi) \to 0$, and in view of Eq. (11.10) $r_m \to 0$. In such a case, the term $1/r_m$ dominates the capillary pressure, P_c, and the total capillary bridge force F_c, see Eqs. (11.5a) and (11.6). Therefore, for small pendular rings ($\psi \to 0$) Eq. (11.7) holds and the toroid approximation can be applied with a good precision.

As already mentioned, other case, in which the toroid approximation works accurately, is that of symmetric nodoid-shaped bridges for $70° < \varphi_c < 90°$, see Eq. (11.54) below. However, to achieve really accurate and reliable numerical results it is preferable to work with the rigorous expressions for the capillary bridge shape, given in the next Section 11.3, and to calculate the capillary bridge force using Eq. (11.2), or its equivalent forms (11.5) and (11.5a).

11.3. GEOMETRICAL AND PHYSICAL PROPERTIES OF CAPILLARY BRIDGES

11.3.1. TYPES OF CAPILLARY BRIDGES AND EXPRESSIONS FOR THEIR SHAPE

Let us define the dimensionless capillary pressure

$$p \equiv P_c r_0 /(2\sigma) \equiv k_1 r_0 \tag{11.14}$$

Here k_1 stands for the mean curvature of the capillary meniscus. The sequence of meniscus shapes, observed when p is increased, has been classified by Plateau [34], see Section 2.2.3 and Table 11.1. The capillary pressure P_c can be both positive and negative; in general $-\infty < p < +\infty$. Note that the presence of "neck" (Fig. 2.6a) not necessarily means that the capillary pressure p is *negative*. Indeed, the catenoid and unduloid, corresponding to $0 \leq p < \frac{1}{2}$ (Table 11.1) have necks, but their capillary pressure is not negative, i.e. the pressure inside the bridge P_1 is equal or greater than the outside pressure P_2. On the other hand, all bridges with a "haunch" (Fig. 2.6b) have *positive* capillary pressure, $\frac{1}{2} < p < \infty$.

Table 11.1. Types of capillary bridges depending on dimensionless capillary pressure $p \equiv P_c r_0/(2\sigma)$; $k_1 \equiv p/r_0$; r_0 is the radius of the "neck" or "haunch"; r_c is contact line radius; L_{nn}, L_{nh}, L_{un}, L_{uh}, L^*, L_c and L_s are upper stability limits; see Eq. (11.16) and Fig. 11.5 for the notation.

bridges with "neck"				bridges with "haunch"		
$-\infty < p < 0$	$p = 0$	$0 < p < 1/2$	$p = 1/2$	$1/2 < p < 1$	$p = 1$	$1 < p < +\infty$
nodoid	catenoid	unduloid	cylinder	unduloid	sphere	nodoid
L_{nn}, see Eq. (11.59)	$L^*/r_c = 1.3255$ $L^*/2r_0 = 1.200$	L_{un}, see Eq. (11.56)	$L_c/2r_0 = \pi$	L_{uh}, see Eq. (11.57)	$L_s/2r_0 = 1$	L_{nh}, see Eq. (11.60)
Notation: $q_1 = (1 - \rho_0^2/\rho_1^2)^{1/2}$, $\sin\phi_1 = q_1^{-1}(1 - \rho_0^2/\rho^2)^{1/2}$ $\varepsilon = -1$ for nodoid, $\varepsilon = +1$ for unduloid			–	Notation: $q_2 = (1 - \rho_1^2/\rho_0^2)^{1/2}$, $\sin\phi_2 = q_2^{-1}(1 - \rho^2/\rho_0^2)^{1/2}$ $\varepsilon = -1$ for nodoid, $\varepsilon = +1$ for unduloid		
Shape: $(\rho_0 \le \rho \le \rho_1)$ $|k_1|z(\rho) = \pm\{\rho_1 E(\phi_1,q_1) + \varepsilon\rho_0 F(\phi_1,q_1) - [(\rho^2 - \rho_0^2)(\rho_1^2 - \rho^2)]^{1/2}/\rho\}$			$r = r_0$	Shape: $(\rho_1 \le \rho \le \rho_0)$ $k_1 z(\rho) = \pm[\rho_0 E(\phi_2,q_2) + (1-\rho_0)F(\phi_2,q_2)]$		
Area: $A(r) = 2\pi \int_{r_0}^{r} dr\, r\, (1 + z_r^2)^{1/2}$ $= \dfrac{2\pi}{k_1^2} \{\rho_1 E(\phi_1,q_1) - [(\rho^2 - \rho_0^2)(\rho_1^2 - \rho^2)]^{1/2}/\rho\}$			$A = 2\pi r_0 z$	Area: $A(r) = 2\pi \int_{r}^{r_0} dr\, r\, (1 + z_r^2)^{1/2}$ $= \dfrac{2\pi}{k_1^2} \rho_0 E(\phi_2,q_2)$		
Volume: $V(r) = \pi \int_{r_0}^{r} dr\, r^2\, dz/dr =$ $= \dfrac{\pi\rho_1}{3\,|k_1^3|}\big|\beta\, E(\phi_1,q_1) - \rho_0^2 F(\phi_1,q_1)$ $- (\beta+\rho^2)[(\rho^2-\rho_0^2)(\rho_1^2-\rho^2)]^{1/2}/(\rho\rho_1)\big|$ $\beta \equiv (2\rho_0^2 + 2\rho_1^2 + 3\varepsilon\rho_0\rho_1)$			$V = = \pi r_0^2 z$	Volume: $V(r) = -\pi \int_{r}^{r_0} dr\, r^2\, dz/dr =$ $= \dfrac{\pi}{3k_1^3}\big|\beta\, \rho_0 E(\phi_2,q_2) - \rho_0\rho_1^2 F(\phi_2,q_2)$ $+ \rho[(\rho^2-\rho_1^2)(\rho_0^2-\rho^2)]^{1/2}\big|$ $\beta \equiv (2\rho_0^2 + 2\rho_1^2 + 3\varepsilon\rho_0\rho_1)$		
Running slope: $\tan\varphi = dz/dr$ $\cos^2\varphi = (\rho^2-\rho_0^2)(\rho_1^2-\rho^2)/\rho^2$			–	Running slope: $\tan\varphi = dz/dr$ $\cos^2\varphi = (\rho^2-\rho_1^2)(\rho_0^2-\rho^2)/\rho^2$		

With the help of Eq. (11.4) one can bring Eq. (11.2) into the form

$$F_c = -2\pi r_0 \sigma (1 - p) \tag{11.15}$$

For a spherical capillary bridge $p = 1$ and Eq. (11.15) gives zero capillary bridge force, $F_c = 0$. The latter means that for a spherical bridge the repulsive capillary pressure force, $F^{(p)} = \pi r_0^2 P_c$, exactly counterbalances the attractive contribution of the surface tension, $F^{(\sigma)} = -2\pi r_0 \sigma$, cf. Eq. (11.2). The fact that if $F_c = 0$, then the capillary bridge must be a zone of sphere, has been established by Mason and Clark [62].

Note also, that the nodoid with "haunch" ($1 < p < \infty$) is the only type of capillary bridge, for which the total capillary-bridge force is repulsive, $F_c > 0$. On the other hand, the nodoid with "neck" is the only type of capillary bridge, for which the capillary pressure is negative, $p < 0$.

To describe the shape of the capillary bridges we will use the same notation as in Section 2.2.3; in addition, we introduce the following dimensionless variables:

$$\rho = |k_1| r, \qquad \rho_0 = |k_1| r_0, \qquad \rho_1 = |k_1| r_1, \quad \rho_c = |k_1| r_c \tag{11.16}$$

In view of Eq. (2.28) one has

$$\rho_1 = |1 - \rho_0 \, \text{sign}(p)| \tag{11.17}$$

where $\text{sign}(p)$ denotes the sign of p. Then Eq. (2.48), which governs the shape of the capillary bridge, can be represented in the form

$$\tan \varphi \equiv \frac{dz}{dr} = \pm \frac{\rho_0 \rho_1 + \varepsilon \rho^2}{\sqrt{(\rho^2 - \rho_0^2)(\rho_1^2 - \rho^2)}} \tag{11.18}$$

Here, as before, φ is the running meniscus slope angle, see Fig. 11.2, and the parameter $\varepsilon = \pm 1$ is defined in Table 11.1. In addition,

$$\rho_0 \leq \rho \leq \rho_1 \qquad \qquad \text{for a bridge with "neck",} \tag{11.19a}$$

$$\rho_1 \leq \rho \leq \rho_0 \qquad \qquad \text{for a bridge with "haunch".} \tag{11.19b}$$

The integration of Eq. (11.18), in view of Eq. (11.16), yields the expressions for the generatrix of the meniscus profile, $z(\rho)$, which are given in Table 11.1; in fact, these expressions are

equivalent to Eqs. (2.50) and (2.52). The elliptic integrals of the first and second kind, $F(\phi, q)$ and $E(\phi, q)$, are defined by Eq. (2.51). In the special case of *catenoid* the meniscus shape is determined by Eq. (2.49). For the catenoid the meridional and azimuthal curvature radii are equal by magnitude, $|r_m| = |r_a|$, as it is for a sphere; however, $r_m = -r_a$. For that reason the surface obtained by a rotation of a catenoid is sometimes termed "pseudosphere". For a sphere the deviatoric curvature $D \equiv 1/r_a - 1/r_m$ is constant, $D \equiv 0$, whereas for a pseudosphere $D = r_0/r^2$, i.e. it is not zero and varies from point to point.

Table 11.1 contains also expressions for the area $A(r)$ and volume $V(r)$ derived with the help of Eq. (11.18). $A(r)$ and $V(r)$ represent, respectively, the meniscus area and the volume of a portion of the bridge confined between the cross-sections of radii r and r_0, the latter being the section across the neck/haunch. With the help of the expressions for $A(r)$ and $V(r)$ given in Table 11.1 one can determine the portions of bridge surface area and volume, $A(r_x, r_y)$ and $V(r_x, r_y)$ comprised between every two sections of radii r_x and r_y,

$$A(r_x, r_y) = |A(r_x) \mp A(r_y)|, \qquad\qquad V(r_x, r_y) = |V(r_x) \mp V(r_y)| \qquad\qquad (11.20)$$

where the signs "−" and "+" stand, respectively, for sections situated on the same and the opposite side(s) with respect to the section $r = r_0$ (the neck/haunch).

11.3.2. RELATIONS BETWEEN THE GEOMETRICAL PARAMETERS

First, let us note that

$$\rho^2 \le \rho_0\rho_1 \qquad\qquad \text{for nodoid with "neck"} \qquad\qquad\qquad (11.21)$$

$$\rho^2 \ge \rho_0\rho_1 \qquad\qquad \text{for nodoid with "haunch"} \qquad\qquad\qquad (11.22)$$

$$\rho^2 = \rho_0\rho_1 \qquad\qquad \text{inflection point for all unduloids} \qquad\qquad (11.23)$$

In addition, from the definition of ε (Table 11.1) and from Eq. (11.17) it follows

$$(\rho_1 + \varepsilon\rho_0)^2 = 1 \qquad\qquad\qquad\qquad\qquad\qquad\qquad\qquad\qquad (11.24)$$

Then using the identity $(\cos\varphi)^{-2} = 1 + \tan^2\varphi$ from Eq. (11.18) one can express the cosine of the running slope angle:

$$\cos^2\varphi = [(\rho^2 - \rho_0{}^2)(\rho_1{}^2 - \rho^2)]/\rho^2 \qquad\qquad\qquad\qquad\qquad (11.25)$$

Equation (11.25), which holds for both nodoids and unduloids, can be represented also in the form

$$(\rho_0\rho_1)^2 - \rho^2(\rho_0^2 + \rho_1^2) + \rho^2\cos^2\varphi + \rho^4 = 0, \tag{11.26}$$

which can be considered as a quadratic equation for determining ρ^2 if ρ_0 and φ are given:

$$\rho^2 = \tfrac{1}{2}[b \pm (b^2 - 4\rho_0^2\rho_1^2)^{1/2}] \tag{11.27}$$

$$b \equiv \rho_0^2 + \rho_1^2 - \cos^2\varphi = \sin^2\varphi - 2\varepsilon\rho_0\rho_1 \tag{11.28}$$

The fact that Eq. (11.27) contains two roots for ρ^2 deserves a special attention.

In the case of *nodoid* ($\rho_0 - \rho_1 = \pm 1$) Eq. (11.27) has always two positive roots for ρ^2, which in view of Eqs. (11.21) and (11.22) correspond to the two types of nodoids:

$$\rho^2 = \rho_0\rho_1 + \tfrac{1}{2}\{\sin^2\varphi - [(\sin^2\varphi + 4\rho_0\rho_1)\sin^2\varphi]^{1/2}\} \quad \text{(nodoid with “neck”)} \tag{11.29}$$

$$\rho^2 = \rho_0\rho_1 + \tfrac{1}{2}\{\sin^2\varphi + [(\sin^2\varphi + 4\rho_0\rho_1)\sin^2\varphi]^{1/2}\} \quad \text{(nodoid with “haunch”)} \tag{11.30}$$

In the case of *unduloid* ($\rho_0 + \rho_1 = 1$) Eq. (11.27) has real roots for ρ^2 only when

$$0 < \rho_0 \le \sin^2\frac{\varphi}{2} \qquad \text{(for unduloid with “neck”, } \varphi < \pi/2) \tag{11.31}$$

$$\sin^2\frac{\varphi}{2} \le \rho_0 < 1 \qquad \text{(for unduloid with “haunch”, } \varphi > \pi/2) \tag{11.32}$$

To understand the meaning of the two roots in the case of unduloids, one can express Eq. (11.27) in the form

$$\rho^2 = \rho_0\rho_1 + \tfrac{1}{2}\{\sin^2\varphi - 4\rho_0\rho_1 \pm [(\sin^2\varphi - 4\rho_0\rho_1)\sin^2\varphi]^{1/2}\} \qquad \text{(all unduloids)} \tag{11.33}$$

Then in view of Eq. (11.23) the two roots in Eq. (11.33) are the radial coordinates of the two points with the same slope angle φ, situated on the left and right from the inflection point of the unduloid at $\rho^2 = \rho_0\rho_1$.

Another possible problem, appearing when the boundary conditions for the meniscus shape are imposed, is to determine the radius of the neck/haunch, ρ_0, for given ρ and φ. With that end in view we use Eq. (11.24) to represent Eq. (11.26) in the form

$$u^2 - 2\varepsilon\rho^2 u + (\rho^4 - \rho^2 \sin^2\varphi) = 0, \qquad\qquad u \equiv \rho_0\rho_1 \qquad\qquad (11.34)$$

Solving Eq. (11.34) for *nodoid*-shaped bridge one obtains $u = \rho^2 \pm \rho\sin\varphi$, where the roots with

"+" and "−" correspond to meniscus with "neck" and "haunch", respectively. Then using the

fact that for nodoid $\rho_1 = \rho_0 \pm 1$, and consequently, $u = \rho_0^2 \pm \rho_0$, one derives

$$\rho_0 = \tfrac{1}{2}\{[1 + 4\rho(\rho + \sin\varphi)]^{1/2} - 1\} \qquad\qquad \text{(nodoid with "neck")} \qquad\qquad (11.35)$$

$$\rho_0 = \tfrac{1}{2}\{[1 + 4\rho(\rho - \sin\varphi)]^{1/2} + 1\} \qquad\qquad \text{(nodoid with "haunch", } \rho > \sin\varphi) \qquad (11.36)$$

Solving Eq. (11.34) for *unduloid*-shaped bridge one obtains $u = -\rho^2 + \rho\sin\varphi$ (the other root

must be disregarded). Since for nodoid $u = \rho_0 - \rho_0^2$, one finally derives

$$\rho_0 = \tfrac{1}{2}\{1 - [1 - 4\rho(\sin\varphi - \rho)]^{1/2}\} \qquad\qquad \text{(unduloid with "neck", } \rho < \sin\varphi), \qquad (11.37)$$

$$\rho_0 = \tfrac{1}{2}\{1 + [1 - 4\rho(\sin\varphi - \rho)]^{1/2}\} \qquad\qquad \text{(unduloid with "haunch", } \rho < \sin\varphi) \quad (11.38)$$

Equations (11.37) and (11.38) yield $0 < \rho_0 < \tfrac{1}{2}$, and $\tfrac{1}{2} < \rho_0 < 1$, respectively, which in view of

Table 11.1 determines the type of the bridge (for unduloids $\rho_0 \equiv p$).

Capillary bridge formed between axisymmetric surface and a plane. To illustrate the

application of the above equations let us consider the capillary bridge formed between a curved

axisymmetric surface of equation $z = h(r)$ and a plane. The equation $z = h(r)$ may represent a

sphere (see Fig. 11.3), or the shape of the cantilever of the atomic force microscope, see Refs.

[23-25, 46]. To specify the problem we assume that the contact angles θ_1 and θ_2 are known

(cf. e.g. Fig. 11.3), and that the capillary pressure P_c is negative, i.e. we deal with a nodoid-

shaped bridge with neck. Such bridges can be spontaneously formed by capillary *condensation*

of water between two *hydrophilic* surfaces at atmospheric humidity lower than 100 %;

alternatively, such bridges can be spontaneously formed by capillary *cavitation* of vapor-filled

bridges between two *hydrophobic* surfaces at temperatures lower than the boiling point of the

aqueous phase; see Section 11.4 for more details. The meniscus slope angle at the curved

surface is

$$\varphi_c = \theta_2 + \arctan(dh/dr) \qquad\qquad\qquad\qquad\qquad\qquad\qquad\qquad\qquad (11.39)$$

Then for a given (dimensionless) contact radius on the *curved* solid surface, $\rho_c = |k_1|r_c$, using Eq. (11.35) one calculates the radius of the neck,

$$\rho_0 = \tfrac{1}{2}\{[1 + 4\rho_c(\rho_c + \sin\varphi_c)]^{1/2} - 1\}, \tag{11.40}$$

of the nodoid-shaped surface; the real bridge meniscus represents a part (zone) of this surface. With the value of ρ_0 thus obtained from Eq. (11.29) one determines the (dimensionless) contact radius $\bar{\rho}_c$ at the *planar* solid surface:

$$\bar{\rho}_c^2 \equiv (k_1\bar{r}_c)^2 = \rho_0\rho_1 + \tfrac{1}{2}\{\sin^2\theta_1 - [(\sin^2\theta_1 + 4\rho_0\rho_1)\sin^2\theta_1]^{1/2}]\} \qquad (\rho_1 = \rho_0 + 1) \tag{11.41}$$

Further, the length of the capillary bridge (the distance between the planes of the contact lines on the curved and planar solid surfaces) can be expressed in the form

$$h(r_c) = |z(\rho_c) \pm z(\bar{\rho}_c)| \tag{11.42}$$

where the function $z(\rho)$ is given in Table 11.1; the sign is "+" or "−" depending on whether the neck appears on the real meniscus, or on its extrapolation; as already mentioned, $h(r)$ is a known function. Having in mind Eqs. (11.40) and (11.41) one concludes that Eq. (11.42) relates two parameters: ρ_c and k_1, or equivalently, $r_c = \rho_c/|k_1|$ and $P_c = 2\sigma k_1$. If one of them (the contact-line radius r_c, or the capillary pressure P_c) is known, then we can determine the other one by solving numerically Eq. (11.42).

Similar procedure can be applied to the case of unduloid with neck; in the latter case one has to use Eqs. (11.37) and (11.33) instead of Eqs. (11.40) and (11.41).

11.3.3. SYMMETRIC NODOID-SHAPED BRIDGE WITH NECK

In this subsection we consider another example of physical importance: nodoid-shaped bridge with neck, formed between two identical parallel planar solid surfaces separated at a distance h (Fig. 11.4). As mentioned earlier, when the liquid phase is water, an aqueous bridge can be formed between two hydrophilic solid surfaces, or alternatively, a vapor-filled bridge can be formed between two hydrophobic solid surfaces. In both cases we will denote by φ_c the meniscus slope angle at the contact line, which represents also the three-phase contact angle
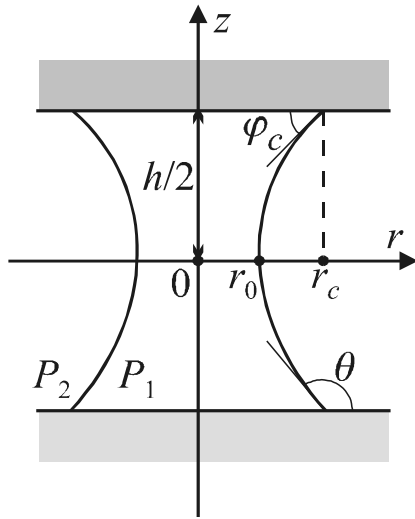
Fig. 11.4. Capillary bridge formed between two plane-parallel solid surfaces separated at a distance h; r_0 and r_c are the radii of the neck and the contact line; φ_c is the contact angle measured across the phase of the bridge.

measured across the phase of the bridge ($\varphi_c < 90°$). As before, $\rho_c = |k_1| r_c$ is the dimensionless radius of the contact line. With the help of Table 11.1 and Eq. (11.25) the equation for the length of the bridge, $h = 2z(\rho_c)$, can be represented in the form

$$|k_1| \, h/2 + \rho_1 E(\phi_1, q_1) = \rho_0 F(\phi_1, q_1) + \cos\varphi_c \qquad (11.43)$$

where

$$q_1 \equiv (1 - \rho_0^2/\rho_1^2)^{1/2}, \qquad \sin\phi_1 \equiv (1 - \rho_0^2/\rho_c^2)^{1/2}/q_1, \qquad \rho_1 = \rho_0 + 1. \qquad (11.44)$$

In view of Eqs. (11.40) and (11.44) one can use Eq. (11.43) to calculate ρ_c if k_1 is known, or *vice versa*, to determine k_1 (and the capillary pressure $P_c = 2\sigma k_1$) if $r_c = \rho_c/|k_1|$ is given. To achieve that one has to solve Eq. (11.43) numerically; the stable numerical method of the "arithmetic-geometric mean" can be applied to calculate the elliptic integrals, see Ref. [63] – Chapter 17.6 therein. Depending on the parameters values Eq. (11.43) could have one or two solutions.

Long ago Plateau [34] established that two solutions are possible for a nodoid-shaped bridge with neck, formed between two parallel circular discs, at given volume, radius r_c and separation h; see also Refs. [59,60]. Experimentally, one of the solutions corresponds to a stable bridge, but loses its stability when it coincides with the other solution, in which case the fluid separates axisymmetrically forming cap-shaped drops onto the two discs [34,59].

Let us now investigate analytically the case $70° < \varphi_c < 90°$, in which the elliptic integrals can be asymptotically expressed in terms of algebraic functions. (Note that in the case of hydrophobic plates gas-filled bridge $70° < \varphi_c < 90°$ corresponds to $90° < \theta < 110°$, where θ is the contact angle measured across *water*, see Fig. 11.4.) In this range of angles, which is often experimentally observed, one has

$$\sin\varphi_c \approx 1 - \eta^2/2, \qquad \eta \equiv \cos\varphi_c, \qquad \eta^2 << 1 \qquad (11.45)$$

The substitution of the latter expression in Eq. (11.40), after expansion in series, yields

$$\rho_0 = \rho_c - \rho_c\eta^2/[2(1 + 2\rho_c)] + O(\eta^4) \qquad (11.46)$$

Then one derives

$$(1 - \rho_0^2/\rho_c^2)^{1/2} = \eta\,(1 + 2\rho_c)^{-1/2} + O(\eta^3) \qquad (11.47)$$

With the help of Eqs. (11.17) and (11.46) one obtains:

$$(1 - \rho_0^2/\rho_1^2)^{1/2} = (1 + 2\rho_c)^{1/2}/(1 + \rho_c) + O(\eta^2) \qquad (11.48)$$

Next, the combination of Eqs. (11.47) and (11.48) yields:

$$\sin\phi_1(\rho_c) \equiv (1 - \rho_0^2/\rho_c^2)^{1/2}\,(1 - \rho_0^2/\rho_1^2)^{-1/2} = \eta\,(1 + \rho_c)/(1 + 2\rho_c) + O(\eta^3) \qquad (11.49)$$

One sees that $\sin\phi_1(\rho_c) = O(\eta)$ is a small quantity. Then the elliptic integrals can be expanded in series:

$$F(\phi_1,q_1) = \int_0^{\sin\phi_1} \frac{d\alpha}{\sqrt{1 - q_1^2 \sin^2\alpha}} \approx \sin\phi_1 + O(\sin^3\phi_1) \approx E(\phi_1,q_1) \qquad (11.50)$$

Eqs. (11.49) and (11.50) lead to

$$F(\phi_1,q_1) \approx E(\phi_1,q_1) \approx \sin\phi_1 = \eta\,(1 + \rho_c)/(1 + 2\rho_c) + O(\eta^3) \qquad (11.51)$$

Finally, the substitution of Eq. (11.51) into Eq. (11.43) yields a simple relation between the thickness of the gap, h, and the dimensionless radius of the contact line ρ_c:

$$h \approx \frac{2\cos\varphi_c}{|k_1|} \frac{\rho_c}{1 + 2\rho_c} \qquad (0 < \rho_c < \infty;\ 70° < \varphi_c < 90°) \qquad (11.52)$$

Note that the above expansions for small η are uniformly valid for $0 < \rho_c < \infty$ and $k_1 < 0$. For $\rho_c \to 0$ (and $k_1 < 0$) Eq. (11.52) gives $h \to 0$, as it could be expected. In the other limit, $\rho_c \to \infty$ Eq. (11.52) reduces to

$$h_{\max} = \frac{\cos\varphi_c}{|k_1|} \qquad\qquad (70° < \varphi_c < 90°) \qquad\qquad (11.53)$$

where $h_{\max}$ denotes the maximum possible length of the bridge (the maximum width of the gap between the plates), for given values of the capillary pressure, $P_c = 2\sigma k_1$, and the contact angle φ_c, the latter being measured across the bridge phase.

It is worth noting that *for fixed h* and $\rho_c \to 0$ Eq. (11.52) gives $k_1 \to 0$, but the ratio $r_c = \rho_c / |k_1|$ $\to h/(2\cos\varphi_c)$ tends to a non-zero constant. One can obtain smaller values of r_c (i.e. $r_c < h/2\cos\varphi_c$) only using unduloid (rather than nodoid) with "neck". It should be also noted, that Eq. (11.52) can be presented in the alternative form

$$-P_c = \sigma \left(\frac{2\cos\varphi_c}{h} - \frac{1}{r_c} \right) \qquad\qquad (70° < \varphi_c < 90°) \qquad\qquad (11.54)$$

The comparison between Eqs. (11.54) and (11.6) shows that the meridional curvature radius is constant: $r_m = -h/(2\cos\varphi_c) = $ const. In fact, Eq. (11.54) represents the result, which would be obtained if the "toroid" ("circle") approximation were directly applied to express the capillary pressure using the definition (11.8b) for the azimuthal curvature radius r_a. Hence, it turns out that the toroid approximation can be applied with a good precision to *nodoid*-shaped bridges with neck, if the contact angle belongs to the interval $70° < \varphi_c < 90°$.

Similar expansion for small η^2 can be applied also to the case of *unduloid* with neck; as a starting point one is to use Eq. (11.37) with $\rho = \rho_c$, instead of Eq. (11.40). In first approximation one obtains again Eq. (11.54), that is the toroid approximation.

11.3.4. GEOMETRICAL AND PHYSICAL LIMITS FOR THE LENGTH OF A CAPILLARY BRIDGE

Although derived for a special type of capillary bridge, Equation (11.53) demonstrates the existence of limits for the length of a capillary bridge. The nodoid and unduloid are periodical curves along the z-axis, see Figs. 2.7 and 11.5. Moreover, the nodoid has self-intersection
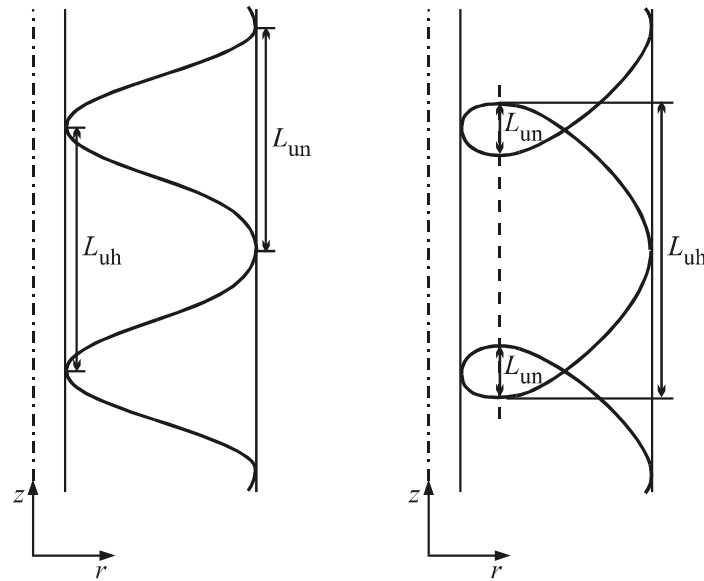
Fig. 11.5. Geometrical upper limits for the stability of capillary bridges: (a) distances between two closest points with vertical tangents for an unduloid with "neck", L_{un}, and with "haunch", L_{uh}; (b) distances between two closest points with horizontal tangents for a nodoid with "neck", L_{nn}, and with "haunch", L_{nh}.

points. Unduloid-shaped bridges of length greater than the period of unduloid as a rule are physically unstable, see Refs. [59,60]; hence the period of unduloid gives an upper limit for the stability of the respective bridges (the longer bridges are unstable, whereas the shorter bridges could be stable or unstable). The distance (along the *z*-axis) between two consecutive points with horizontal tangent (slope angle $\varphi = 0$) on the nodoid (Fig. 11.5b) can also serve as an upper limit for the stability of nodoid-shaped bridges. Below we provide expressions for these upper stability limits, which could be helpful for estimates.

In Fig. 11.5a the geometrical limits for the stability of the unduloids with "neck" and "haunch" are denoted by L_{un} and L_{uh}, respectively. Each of them can be identified with $2z(\rho_1)$, where the function $z(\rho)$ is given in Table 11.1. In addition, for $\rho = \rho_1$ one has $\sin\phi_1 = \sin\phi_2 = 1$; consequently, $\phi_1 = \phi_2 = \pi/2$, and the elliptic integrals in Table 11.1 reduce to the respective total elliptic integrals [63-66]:

$$\mathbf{K}(q) \equiv \mathrm{F}(\pi/2, q), \qquad \mathbf{E}(q) \equiv \mathrm{E}(\pi/2, q), \qquad (11.55)$$

Then with the help of Eqs. (11.14), (11.16), (11.17) and the expressions for $z(\rho)$ in Table 11.1 one obtains

$$L_{\text{un}}(p)/(2r_0) = \mathbf{K}(q_1) + \frac{1-p}{p}\,\mathbf{E}(q_1), \qquad q_1 = \frac{\sqrt{1-2p}}{1-p} \qquad \text{for } 0 < p < \tfrac{1}{2} \qquad (11.56)$$

$$L_{\text{uh}}(p)/(2r_0) = \mathbf{E}(q_2) + \frac{1-p}{p}\,\mathbf{K}(q_2), \qquad q_2 = \frac{\sqrt{2p-1}}{p} \qquad \text{for } \tfrac{1}{2} < p < 1 \qquad (11.57)$$

For $p \to \tfrac{1}{2}$ one has $q_1 = q_2 = 0$; in addition, $\mathbf{K}(0) = \mathbf{E}(0) = \pi/2$. Then from Eqs. (11.56) and (11.57) one obtains

$$L_{\text{c}} \equiv \lim_{p \to 1/2} L_{\text{un}}(p) = \lim_{p \to 1/2} L_{\text{uh}}(p) = 2\pi r_0 \qquad (11.58)$$

Indeed, the upper limit for the stability of a *cylindrical* ($p = \tfrac{1}{2}$) capillary bridge of radius r_0 is $L_{\text{c}} = 2\pi r_0$. This critical value was given first by Beer [67] and obtained in the studies by Plateau [34]. $L_{\text{c}} = 2\pi r_0$ is the limit of stability of the cylindrical bridge against axisymmetric perturbations at fixed (controlled) *volume* of the bridge. In the case of *pressure* control the limit of stability appears at two times shorter length: $L = \pi r_0$, see e.g. Refs. [59,60].

For $p \to 1$ (spherical bridge, Table 11.1) Eq. (11.57) yields $L_{\text{uh}} \to 2r_0$; indeed, from geometrical viewpoint the larger possible diameter of a spherical bridge is the diameter of the sphere, $2r_0$.

The geometrical limits for the length of a nodoid-shaped bridge (see Fig. 11.5b) can be determined in a similar way:

$$\frac{L_{\text{nn}}}{2r_0} = \mathrm{F}(\phi_{1g}, q_{1g}) + \frac{\sqrt{2|p|+1}}{|p|} - \frac{|p|+1}{|p|}\mathrm{E}(\phi_{1g}, q_{1g}) \qquad -\infty < p < 0 \qquad (11.59)$$

$$\frac{L_{\text{nh}}}{2r_0} = \mathrm{E}(\phi_{2g}, q_{2g}) - \frac{p-1}{p}\mathrm{F}(\phi_{2g}, q_{2g}) \qquad 0 < p < \infty \qquad (11.60)$$

where $q_{1g} \equiv (2|p|+1)^{1/2}(1+|p|)^{-1}$; $\sin\phi_{1g} \equiv [(1+|p|)/(2|p|+1)]^{1/2}$; $q_{2g} \equiv (2p-1)^{1/2}p^{-1}$ and $\sin\phi_{2g} \equiv [p/(2p-1)]^{1/2}$; the fact that the nodoid has horizontal tangent at $\rho = \rho_g \equiv (\rho_0\rho_1)^{1/2}$ has been used. For $p \to 1$ Eq. (11.60) yields $L_{\text{nh}} \to 2r_0$, i.e. we arrive again to the result for a sphere, see above.

For $p \to 0$ Eqs. (11.56) and (11.59) give divergent values for L_{un} and L_{nn}; this result can be attributed to the fact that there are no geometrical limitations for the length of a *catenoid*. On the other hand, there are physical limitations for the length of a catenoid stemming from the

boundary conditions for the Laplace equation. Plateau [34] produced a catenoid in stable equilibrium by suspending oil on two circular rings and adjusting the volume of the oil so that the interface across the rings was planar. He found that the catenoid thus produced was at the limit of its stability when the distance apart of the rings L to the diameter $2r_c$ reached a value approximately 0.663. He recognized also that for $L/2r_c < 0.663$ there is an alternative catenoid solution not observable in the experiments, and that the limit of stability is reached when the two solutions coincide; see Ref. [59] for more information.

To elucidate this point one can use the equation of the catenoid, Eq. (2.49), to obtain the connection between the length of the bridge, L, and the contact radius r_c:

$$r_c/r_0 = \cosh(L/2r_0) \qquad (11.61)$$

Introducing variables $x \equiv L/2r_0$ and $a \equiv L/2r_c$ one transforms Eq. (11.61) to read

$$x = a \cosh x \qquad (11.62)$$

When a is small enough the straight line $y_1(x) = x$ has two intersection points with the curve $y_2(x) = a \cosh x$; they represent the two roots of Eq. (11.62) corresponding to the two catenoids recognized by Plateau. For larger values of a Eq. (11.62) has no solution. For some intermediate critical value $a = a^*$ the line $y_1(x)$ is tangential to the curve $y_2(x)$ and the two roots coincide; from the condition for identical tangents, $y_1{}'(x^*) = y_2{}'(x^*)$, one obtains $a^* \sinh x^* = 1$. The combination of the last result with Eq. (11.62) yields a transcendental equation for x^* :

$$x^* = \coth x^* \qquad \Rightarrow \qquad x^* \equiv L^*/2r_0 = 1.1996786... \qquad (11.63)$$

Finally, one recovers the result of Plateau: $L^*/2r_c \equiv a^* = (\sinh x^*)^{-1} = 0.6627434... \approx 0.663$. The latter value determines the maximum length, L^*, of the catenoid formed between two identical circular rings of a given radius r_c.

Stability of capillary bridge menisci. As mentioned above, the parameters L_{un}, L_{uh}, L_c, L_{nn}, L_{nh} and L^* calculated above serve as upper limits for the length of the bridges: the longer bridges are unstable, but the shorter bridges could be stable or unstable, depending on the specific conditions. In general, the bridges are more stable when the volume of the bridge and the position of the three-phase contact line are fixed. The bridges are less stable when the pressure, rather than the volume, is fixed; see Refs. [59, 60] for a detailed review.

In general, two methods are used to investigate the stability of capillary bridges. As demonstrated in Section 2.1.2 the Laplace equation of capillarity corresponds to an extremum of the grand thermodynamic potential Ω. A solution of Laplace equation describes a stable or unstable equilibrium meniscus depending on whether it corresponds, respectively, to a minimum or maximum of Ω. Then the sign of the second variation of Ω is an indication for stability or instability. This approach was applied to capillary bridges by Howe [68], and utilized by many authors [69-71].

The second method for determining the stability of capillary menisci arose from the analysis of the behavior of pendant and sessile drops and bubbles used in the methods for surface tension measurements. These observations revealed that the stability limits always lie at *turning points* in the plots of volume against pressure (*PV*-diagrams) [60]. The turning points in *volume* are the points on the *PV*-diagram at which the volume has local minimum or maximum; they represent stability limits in the case of fixed (controlled) volume. Likewise, the turning points in *pressure* are the points on the *PV*-diagram at which the pressure has local minimum or maximum; they represent stability limits in the case of fixed (controlled) pressure.

Classical example for turning points in pressure are the local extrema of pressure in the *PV*-diagram predicted by the well-known van der Waals equation of state for temperatures below the critical one; these turning points separate the unstable region from the region of (meta)stable gas or liquid, see e.g. Ref. [72]. Another example for turning point in pressure is observed with the known "maximum bubble pressure method" for measurement of dynamic surface tension [73-75]; the transition from stability to instability occurs when the bubble reaches hemispherical shape and maximum pressure [76]. Note, however, if the same system is under volume control (say liquid drop of controlled volume instead of bubble) the turning point in pressure is no more a stability limit: stable states beyond hemisphere can be realized. The idea that stability changes for drops *always occur at turning points* was put forward as a proposition for meniscus stability analysis by Padday & Pitt [77] and Boucher & Evans [78]. In addition, bifurcation points on the *PV*-diagrams are also recognized as stability limits, especially for relatively long capillary bridges at volume control (the bridges under pressure control are less stable and cannot survive until the appearance of bifurcation points), see Refs. [60,79] for details.
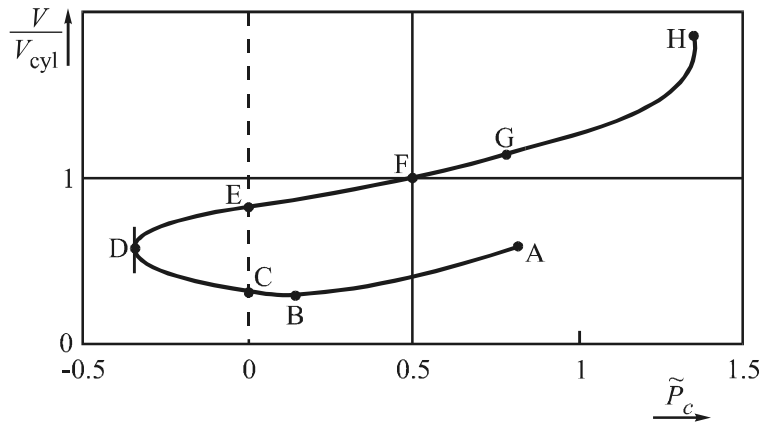
Fig. 11.6. Plot of the volume of a liquid bridge, V, scaled with the volume of the cylindrical bridge, V_{cyl}, against the dimensionless pressure difference across the meniscus surface, $\widetilde{P}_c$, see Eq. (11.64); the bridge is symmetric like that in Fig. 11.4; V and $\widetilde{P}_c$ vary at fixed contact line radius r_c and fixed length L of the bridge {after Ref. [60]}.

For example, the stability limit $L = \pi r_0$ for cylindrical bridge under pressure control is a turning point in pressure, whereas the stability limit $L = 2\pi r_0$ for cylinder under volume control is a bifurcation point [59,60].

Figure 11.6 represents a sketch of a typical *PV*-diagram for relatively short liquid capillary bridges, $L/r_c \le L*/r_c = 1.3255$, which are symmetric with respect to the plane of the "neck"/ "haunch", like it is in Fig. 2.6. Moreover, it is assumed that the contact radius, r_c, is *fixed*, but the slope angle at the contact line, φ_c, can vary, cf. Fig. 11.4. The dimensionless pressure in Fig. 11.6 is defined as follows:

$$\widetilde{P}_c \equiv P_c\, r_c/(2\sigma) \tag{11.64}$$

For catenoid and cylinder $\widetilde{P}_c = p = 0$ and $\frac{1}{2}$, respectively, but in general $\widetilde{P}_c \ne p$, cf. Eqs. (11.14) and (11.64) (p is not suitable to be plotted on a *PV*-diagram, because it reflects not only variations of the pressure P_c, but also changes in the neck radius r_0). Each point on the curve in Fig. 11.6 corresponds to a capillary bridge in mechanical equilibrium, which could be stable or unstable. In particular, the section AB corresponds to unduloid-shaped bridges ($0 < p < \frac{1}{2}$, cf. Table 11.1) with a very thin neck, which are unstable [60]. At the point A the neck radius r_0 becomes zero and the bridge splits on two pieces of spheres. Point B is a turning point in volume; it represents a boundary between stable bridges of controlled volume (on the left) and

the unstable bridges (on the right). Likewise, point D is a turning point in pressure: the whole line DEFGH corresponds to stable bridges under pressure (or volume) control, whereas the section DA corresponds to bridges unstable under pressure control. The section BD represents bridges with neck, which are stable under volume control, but unstable under pressure control. The points C and E, at which $\widetilde{P}_c = p = 0$, represent the two catenoids, determined by the roots of Eq. (11.62). The catenoid bridge E (that of greater volume) is stable in both the regimes of fixed volume and pressure, whereas the catenoid bridge C (that of smaller volume) is stable only in the regime of fixed volume [60]. When $L/r_c = L*/r_c = 1.3255$ points C and E merge with point D, and for $L/r_c > 1.3255$ there are no equilibrium catenoid (and nodoid with neck) bridges. The section EF corresponds to stable unduloid-shaped bridges with "neck" ($0 < p < \frac{1}{2}$), the section FG represents stable unduloid-shaped bridges with "haunch" ($\frac{1}{2} < p < 1$), and finally, the section GH corresponds to stable nodoid-shaped bridges with "haunch" ($p > 1$, cf. Table 11.1). The equilibrium bridges at the points F and G have the shape of cylinder and truncated sphere, respectively. At the point H one has $L/r_0 = L_{nh}/r_0$, see Eq. (11.60), which is the limit of stability of the menisci with "haunch" [60].

For $L/r_c = \pi$ the point F (cylindrical bridge) coincides with the point D (turning point in pressure) and the cylindrical bridge loses its stability under regime of pressure control. For $L/r_c > \pi$ the regions with stable bridges on the PV-diagrams become more narrow, and the PV-diagrams (representing mostly unstable states) become more complicated, see the review by Lowry and Steen [60].

11.4. NUCLEATION OF CAPILLARY BRIDGES

11.4.1. THERMODYNAMIC BASIS

The thermodynamics of nucleation (creation of a new phase from a supersaturated mother phase), stems from the works of Gibbs [80] and Volmer [81], and describes the formation and growth of small clusters from the new phase (drops, bubbles, crystals) in a process of phase transition like condensation of vapors, cavitation (formation of bubbles) in boiling liquids, precipitation of a solute from solution, etc. [82-86]. As a driving force of nucleation the

increased chemical potential of the molecules in the mother phase with respect to the new phase is recognized. The nuclei of the new phase in the processes of *homogeneous* (bulk) condensation and cavitation are spherical drops and bubbles. On the other hand, in the case of *heterogeneous* nucleation (nucleation on a surface) the nuclei have the shape of truncated spheres. In both cases the presence of a *convex spherical* liquid interface of large curvature (small nucleus) leads to a large value of the pressure inside the nucleus, which in its own turn increases the molecular chemical potential with respect to its value in a large phase of planar interface. That is the reason why a necessary condition for such nuclei to appear is the initial phase to be "supersaturated": in the case of condensation the humidity must be slightly above 100 %; in the case of cavitation (boiling) the equilibrium vapor pressure of the liquid to be higher than the applied outer pressure.

The nodoid-shaped capillary bridges (as well as the concave spherical menisci in capillaries) have *negative* capillary pressure and provide quite different conditions for nucleation. Formation of nuclei with such interfacial shape makes possible the condensation to occur at humidity markedly below 100% and the cavitation to happen when the equilibrium vapor pressure of the liquid is considerably lower than the outer pressure. The effect of concave menisci on nucleation was first established in the phenomenon capillary condensation, which appears as a hysteresis of adsorption in porous solids [17, 86-88]. The experiments of McFarlane and Tabor [1] on the adhesion of spherical beads to glass plate in humid atmosphere give an example for nucleation of *liquid* capillary bridges.

The formation of nodoid-shaped *cavities* between two solid surfaces was examined by Yushchenko et al. [89] and Parker et al. [90]. As already mentioned, the formation of such cavities is proposed as an explanation of the attractive hydrophobic surface force [26-31].

As a physical example let us consider the nucleation of nodoid-shaped capillary bridges in the narrow gap between two parallel plates (Fig. 11.4). The theoretical treatment is the same for *liquid* bridges between two hydrophilic solid surfaces and for *gas* bridges between two hydrophobic solid surfaces. In other words, the approach can be applied to both capillary condensation and capillary cavitation. The work of formation of a nucleus can be expressed in the form [82, 83, 85]:

$$W(r_c) = A_l\sigma - 2A_c\sigma\cos\varphi_c - V^{(n)}[P^{(n)}(r_c) - P] + N^{(n)}[\mu^{(n)}(r_c) - \mu] \tag{11.65}$$

which represents the difference between the free energies of the system in the states with and without nucleus. The meaning of the symbols and terms in Eq. (11.65) is the following. As usual, σ is the surface tension, A_l denotes the area of the liquid meniscus and

$$A_c = \pi r_c^2 \tag{11.66}$$

is the area encircled by each of the two contact lines of radius r_c (Fig. 11.4). We will use r_c as a parameter which identifies the capillary bridge, just as in the theory of homogeneous nucleation the drop/bubble radius is used to identify the spherical nuclei. The first and the second terms in the right-hand side of Eq. (11.65) represent the work of formation of new phase boundaries liquid/gas and solid/fluid, respectively; the third term is the mechanical work related to the change in the pressure inside the nucleus, $P^{(n)}$, in comparison with the pressure P in the ambient mother phase; $\mu^{(n)}(r)$ and μ are chemical potentials of the molecules in the nucleus and in the ambient mother phase; $N^{(n)}$ and $V^{(n)}$ are the number of molecules in the nucleus and its volume. We assume that the mechanical equilibrium has been attained (the Laplace and Young equations are satisfied); however, the bridges could be out of chemical equilibrium. In particular, the multiplier $-\sigma\cos\varphi_c$ in Eq. (11.65) stems from the Young equation. As in Section 11.3.3 angle φ_c is the three-phase contact angle measured across the bridge phase (in the case of gas-in-liquid bridge the complementary angle, $\theta = \pi - \varphi_c$, is traditionally called 'the contact angle'). Depending on whether we deal with gas (vapor) or liquid bridges, the following expressions are to be substituted:

$$N^{(n)}[\mu^{(n)}(r_c) - \mu] = P^{(n)}(r_c)V^{(n)}\ln[P^{(n)}(r_c)/P_0] \qquad \text{(gas bridges)} \quad (11.67)$$

$$N^{(n)}[\mu^{(n)}(r_c) - \mu] = (V^{(n)}/V_m)\{[P^{(n)}(r_c)-P]V_m - kT\ln(P'/P_0)\} \qquad \text{(liquid bridges)} \quad (11.68)$$

As before, $P^{(n)}$ is the pressure in the nucleus (in the capillary bridge); P_0 is the equilibrium vapor pressure of a planar liquid surface at that temperature; P' is the vapor pressure in the gas phase surrounding a liquid-bridge nucleus; V_m is the volume per molecule in the liquid phase.

To obtain Eq. (11.67) we have used the expression for the chemical potential of the vapors inside the nucleus, $\mu^{(n)}(r_c) = \mu_0 + kT\ln P^{(n)}(r_c)$, and that for the vapors which are in equilibrium

with the mother phase, $\mu = \mu_0 + kT \ln P_0$; μ_0 is a standard chemical potential; the ideal gas equation, $P^{(n)}(r_c)V^{(n)} = N^{(n)}kT$, has been also employed.

To obtain Eq. (11.68) we have used the expressions $\mu = \mu_0 + kT \ln P'$ and $\mu^{(n)}(r_c) = \mu_0 + kT \ln P^{(v)}(r_c)$, where the equilibrium vapor pressure of the concave liquid bridge, $P^{(v)}$, is given by the Gibbs-Thomson equation

$$P^{(v)} = P_0 \exp(P_c V_m/kT) = P_0 \exp\{ [P^{(n)}(r_c) - P]V_m / kT \} \tag{11.69}$$

Note that quantities like P, P_0, P', μ, V_m, are independent of r_c.

Let us now investigate the dependence of nucleation work W on r_c. Using the Gibbs-Duhem equation for the phase of the bridge, one can write:

$$-V^{(n)}dP^{(n)}/dr_c + N^{(n)}d\mu^{(n)}/dr_c = 0 \tag{11.70}$$

Differentiating Eq. (11.65), along with Eqs. (11.66) and (11.70) one can derive

$$\frac{dW}{dr_c} = \sigma \frac{dA_l}{dr_c} - 4\pi r_c \sigma \cos\varphi_c + [P - P^{(n)}(r_c)]\frac{dV^{(n)}}{dr_c} + [\mu^{(n)}(r_c) - \mu]\frac{dN^{(n)}}{dr_c} \tag{11.71}$$

The meniscus area and the volume of the bridge can be expressed in the form

$$A_l = 2\pi \int_{-h/2}^{h/2} dz\ r(z)(1 + r_z^2)^{1/2} \qquad\qquad V^{(n)} = \pi \int_{-h/2}^{h/2} dz\ r^2(z) \tag{11.72}$$

where $r(z)$ expresses the meniscus profile in cylindrical coordinates and $r_z \equiv \partial r/\partial z$. Note, that in general the meniscus profile depends on r_c through the boundary condition at the contact line; in other words $r = r(z,r_c)$. Differentiating under the sign of the integrals in Eq. (11.72) and using integration by parts one can prove that

$$\sigma \frac{dA_l}{dr_c} + [P - P^{(n)}(r_c)]\frac{dV^{(n)}}{dr_c} =$$

$$= 2\pi \int_{-h/2}^{h/2} dz\, r \frac{\partial r}{\partial r_c}\left[\frac{1}{r(1+r_z^2)^{1/2}} - \frac{r_{zz}}{(1+r_z^2)^{3/2}} + \frac{P - P^{(n)}}{\sigma} \right] + 4\pi r_c \sigma \cos\varphi_c \tag{11.73}$$

where $r_{zz} \equiv \partial^2 r/\partial z^2$. The expression in the brackets must be equal to zero because the meniscus shape $r(z)$ obeys the Laplace equation, Eq. (2.23). Then substituting Eq. (11.73) into Eq. (11.71) one obtains

$$\frac{dW}{dr_c} = [\mu^{(n)}(r_c) - \mu]\frac{dN^{(n)}}{dr_c} \tag{11.74}$$

In the theory of nucleation [81-86] the critical nucleus is defined as the nucleus with maximum *W*. Then for the critical nucleus $dW/dr_c = 0$ and from Eq. (11.74) one obtains

$$\mu^{(n)}(r_c*) = \mu \tag{11.75}$$

that is the critical nucleus of contact radius $r_c = r_c*$ is in chemical equilibrium with the ambient mother phase. In view of Eqs. (11.67) and (11.68) this yields

$$P^{(n)}(r_c*) = P_0 \qquad\qquad \text{(gas bridge)} \tag{11.76}$$

$$P^{(n)}(r_c*) = P - (kT/V_m)\ln(P_0/P') \qquad\qquad \text{(liquid bridge)} \tag{11.77}$$

P is to be identified with the atmospheric pressure. Below the boiling temperature of the liquid (say at room temperature) one has $P^{(n)}(r_c*) = P_0 < P$ for a gas bridge; likewise, the capillary condensation usually takes place at humidity below 100 %, i.e. $P'/P_0 < 1$ and then Eq. (11.77) gives also $P^{(n)}(r_c*) < P$. As mentioned earlier, a negative pressure difference, $P^{(n)}(r_c*) - P < 0$, can be attained only in capillary bridges with generatrix nodoid ($-\infty < p < 0$, see Table 11.1).

11.4.2. CRITICAL NUCLEUS AND EQUILIBRIUM BRIDGE

The dependence $W = W(r_c)$ can be calculated in the following way. For given values of ρ_c, *h* and φ_c, from Eqs. (11.40) and (11.43) one calculates ρ_0 and k_1. The substitution of the results in the expressions for the area and volume of *nodoid*-shaped bridge with neck (Table 11.1) give $A_l(r_c)$ and $V^{(n)}(r_c)$, where $r_c = \rho_c/|k_1|$. Further, in view of Eq. (11.14) the capillary pressure is $[P - P^{(n)}(r_c)] = 2\sigma|k_1|$. Finally, a substitution of the results in Eqs. (11.65)–(11.68) gives $W(r_c)$. For the smallest values of r_c the (non-equilibrium) bridges are *unduloids* with neck, for which $W(r_c)$ can be calculated in a similar way, but Eq. (11.37) with $\rho = \rho_c$ must be used instead of Eq. (11.40).

Physical interest represent situations, in which $h < h_{max}$, where h_{max} denotes the maximum possible length of the bridge, see Fig. 11.4. For $70° < \varphi_c < 90°$ one can estimate h_{max} with the help of Eq. (11.53). For example, let us consider the case of nucleation of vapor-filled bridges

Table 11.2. Values of the maximum possible length, h_{max}, of a vapor-filled equilibrium capillary bridge between two hydrophobic plates in water as a function of the contact angle θ (Fig. 11.4) at temperature 20°C, as predicted by Eq. (11.78).

$\theta = \pi - \varphi_c$	90°	94°	98°	102°	106°	110°
h_{max} (nm)	0	103	205	306	405	503

in water at temperature 20°C. In this case the surface tension is σ = 72.75 mN/m and the equilibrium vapor pressure of water is P_0 = 2337 Pa, which is only 2.3 % of the normal atmospheric pressure at the sea level, P = 101 325 Pa. Equation (11.53) acquires the form

$$h_{max} = \frac{2\sigma\cos\varphi_c}{P - P_0} \qquad\qquad (70° < \varphi_c < 90°) \qquad\qquad (11.78)$$

Table 11.2. contains numerical results for h_{max} calculated with the above parameters values. One sees that h$_{max}$ markedly increases when the contact angle θ of the hydrophobic plate increases beyond 90°. It is worthwhile noting that h_{max} is obtained from Eq. (11.52) for $\rho_c \to \infty$, that is the limit for a large bridge, whose azimuthal curvature radius is much greater than the meridional one, $r_a \gg r_m$. For such bridges $r_m = -h/(2\cos\varphi_c)$ and using Eq. (11.7) one obtains that the length of the bridge is given again by Eq. (11.78) for every $\varphi_c \in [0°, 90°]$ (that is 90° $\leq$ $\theta \leq$ 180°). In this way Table 11.2 can be extended for $\theta >$ 110°; then the maximum possible value of the gap width, corresponding to θ = 180°, is h_{max} = 1470 nm.

The large equilibrium bridges (for which $r_a \gg r_m$) can be considered as a result of the process of nucleation, which begins with a fluctuational formation of much smaller capillary bridges. In the theory of nucleation the small nuclei are generally out of chemical equilibrium with the mother phase, and this is the reason why they could spontaneously grow owing to the addition of new molecules to the nucleus.

A typical picture, originating from the theory of homogeneous condensation (and cavitation), is that a *critical* drop (bubble) exists, corresponding to a maximum of the work of nucleation W, i.e. to a state of unstable equilibrium, see e.g. Refs. [85,86]. If a molecule is added to the critical nucleus it begins to grow spontaneously; on the contrary, if a molecule is detached from the critical nucleus, it spontaneously diminishes and disappears. For example, in the case of

homogeneous condensation of water vapors at 0°C and $P'/P_0 = 4$ the radius of the critical droplet was calculated to be about 0.85 nm [91, 86].

Let us consider now the case of nucleation (condensation or cavitation) of capillary bridges in a narrow gap. The condition for extremum (maximum or minimum) of W determines uniquely the pressure inside the (critical or equilibrium) nucleus, $P^{(n)}$, see Eqs. (11.76) and (11.77), and the value of the parameter $k_1 = [P^{(n)} - P]/(2\sigma)$. Then the number of the extrema of W is equal to the number of roots of Eq. (11.43) for the respective value of k_1 and for the given thickness of the gap, h, and contact angle φ_c. A maximum of W for some value of r_c can be interpreted as existence of a critical nucleus in a state of *unstable* equilibrium with the ambient mother phase. A local minimum of $W(r_c)$ corresponds to a capillary bridge in state of *stable* equilibrium.

Additional information about the nucleation of liquid and gas capillary bridges can be found in Refs. [90, 92].

11.5. SUMMARY

The role of capillary bridges has been recognized to be important for many systems and phenomena such as adhesion of particles (dust, powders) to solid surfaces, consolidation of granules and porous media, dispersion of pigments and wetting of powders, obtaining of latex films, antifoaming, capillary condensation, bridging force in experiments with atomic force microscope (AFM), attraction between hydrophobic surfaces, etc.

The capillary bridge force is oriented normally to the plane of the three-phase contact line and its magnitude is determined by the contributions of the capillary pressure and the normally resolved surface tension force, see Eq. (11.5). The simplest way to quantify the shape of the capillary bridges and the capillary-bridge force is to use the toroid (circle) approximation (Section 11.2.2). Like every approximation it has some limits of validity; moreover, there is an ambiguity in the definition of the azimuthal radius of curvature, which results in different expressions for the capillary bridge force, see Eqs. (11.8) and (11.11). For that reason more reliable results can be obtained using the exact profile of the capillary bridge, which is determined by the Plateau sequence of shapes: (1) nodoid with "neck", (2) catenoid, (3) unduloid with "neck", (4) cylinder, (5) unduloid with "haunch", (6) sphere and (7) nodoid with

"haunch". The capillary-bridge force is attractive for the shapes (1-5), zero for sphere (6) and repulsive for the nodoid (7).

Expressions for the bridge shape, area and volume are given in Table 11.1. In addition, equations connecting the radius of the bridge neck/haunch with the contact angle and radius are derived in Section 11.3.2. For the reader's convenience the procedures for shape calculations are outlined for the cases of bridges between plane and axisymmetric body, and between two parallel planes, see Eqs. (11.39)–(11.44). It is demonstrated that in the asymptotic case, in which the contact angle belongs to the range $70° < \varphi_c < 90°$ (or $90° < \theta < 110°$ for hydrophobic plates), the elliptic integrals reduce to elementary algebraic functions and the capillary bridge can be described in terms of the toroid approximation, see Eqs. (11.52)–(11.54).

Some upper "geometrical" stability limits for the length of the capillary bridges are related to the distances between the points with horizontal and vertical tangents of the nodoid and unduloid, see Eqs. (11.56)–(11.69). The limits for the length of a catenoid-shaped bridge are connected with the possibility to satisfy the boundary conditions with this special shape, see Eq. (11.63). The real "physical" limits for the bridge stability can be established by analysis of diagrams of volume vs. pressure, see Fig. 11.6 and its interpretation.

Finally, we consider the thermodynamics of nucleation of capillary bridges between two solid surfaces. Two plane-parallel plates are considered as an example. The treatment is similar for liquid bridges between two hydrophilic plates and for gas bridges between two hydrophobic plates; in both cases the work of nucleation is determined by Eq. (11.65). Nucleation of capillary bridges is possible when the distance between the plates is smaller than a certain limiting value h_{max}, see Eq. (11.78) and Table 11.2. Equations for calculating the work of nucleation and the size of the critical (and/or equilibrium) nucleus are presented.

11.6.   REFERENCES

1.   J.S. McFarlane, D. Tabor, Proc. R. Soc. London A, 202 (1950) 224.
2.   H.M. Budgett, Proc. R. Soc. London A, 86 (1912) 25.
3.   W. Stone, Phil. Mag. 9 (1930) 610.
4.   F.M. Orr, L.E. Scriven, A.P. Rivas, J. Fluid Mech. 67 (1975) 723.
5.   W.B. Haines, J. Agric. Sci. 15 (1925) 529.

6. W.B. Haines, J. Agric. Sci. 17 (1927) 264.

7. R.A. Fisher, J. Agric. Sci. 16 (1926) 492.

8. P.C. Carman, J. Phys. Chem. 57 (1953) 56.

9. A.D. Zimon, Adhesion of Dust and Powder, Plenum, London, 1969.

10. J. Woodrow, H. Chilton, R.I. Hawes, J. Nucl. Energy B, Reactor Tech. 2 (1961) 229.

11. W.D. Kingery, J. Appl. Phys. 30 (1959) 301.

12. R.B. Heady, J.W. Cahn, Met. Trans. 1 (1970) 185.

13. D.P. Sheetz, J. Polymer Sci. 9 (1965) 3759.

14. J.W. Vanderhoff, H.L. Tarkowski, M.C. Jenkins, E.B. Bradford, J. Macromolec. Chem. 1 (1966) 361.

15. A.S. Dimitrov, T. Miwa, K. Nagayama, Langmuir 15 (1999) 5257.

16. R. Defay, I. Prigogine, in: Surface Tension and Adsorption, Wiley, New York, 1966; p. 217.

17. D.H. Everett, in: E.A. Flood (Ed.) The Solid-Gas Interface, Vol. 2, M. Dekker, New York, 1967; p. 1055.

18. J.C. Melrose, J. Colloid Interface Sci. 38 (1972) 312.

19. M. Iwamatsu, K. Horii, J. Colloid Interface Sci. 182 (1996) 400.

20. N.R. Morrow, J. Can. Pet. Tech. 10 (1971) 38.

21. S.M. Iveson, J.D. Lister, Powder Technol. 99 (1998) 234.

22. S.M. Iveson, J.D. Lister, Powder Technol. 99 (1998) 243.

23. C.M. Mate, V.J. Novotny, J. Chem. Phys. 94 (1991) 8420.

24. O.P. Behrend, F. Oulevey, D. Gourdon, E. Dupas, A.J. Kulik, G. Gremaud, N.A. Burnham, Applied Physics A, 66 (1998) S219.

25. H. Suzuki, S. Mashiko, Applied Physics A, 66 (1998) S1271.

26. H.K. Christenson, J. Fang, J.N. Israelachvili, Phys. Rev. B, 39 (1989) 11750.

27. V.S.J. Carig, B.W. Ninham, R.M. Pashley, J. Phys. Chem. 97 (1993) 10192.

28. W.A. Ducker, Z. Xu, J.N. Israelachvili, Langmuir 10 (1994) 3279.

29. J.C. Eriksson, S. Ljunggren, Langmuir 11 (1995) 2325.

30. V.V. Yaminsky, Colloids Surf. A, 129-130 (1997) 415.

31. V.V. Yaminsky, Langmuir 13 (1997) 2.

32. J. Plateau, Experimental and Theoretical Researches on the Figures of Equilibrium of a Liquid Mass Withdrawn from the Action of Gravity, in: The Annual Report of the Smithsonian Institution, Washington D.C., 1863; pp. 207-285.

33. J. Plateau, The Figures of Equilibrium of a Liquid Mass, in: The Annual Report of the Smithsonian Institution, Washington D.C., 1864; pp. 338-369.

34. J. Plateau, Statique Expérimentale et Théoretique des Liquides Soumis aux Seules Forces Moléculaires, Gauthier-Villars, Paris, 1873.

35. Lord Rayleigh, Proc. London Math. Soc. 10 (1879) 4.

36. Lord Rayleigh, Proc. R. Soc. London 29 (1879) 71.

37. Lord Rayleigh, Philos. Mag. 34 (1892) 145.

38. Lord Rayleigh, Philos. Mag. 34 (1892) 177.

39. N.L. Cross R.G. Picknett, Particle Adhesion in the Presence of a Liquid Film, in: H.R. Johnson and D.H. Litter (Ed.) The Mechanism of Corrosion by Fuel Impurities, Butterworths, London, 1963; p. 383.

40. G. Mason, W.C. Clark, Chem. Eng. Sci. 20 (1965) 859.

41. W.C. Clark, J.M. Haynes, G. Mason, Chem. Eng. Sci. 23 (1968) 810.

42. M.A. Erle, D.C. Dyson, N.R. Morrow, AIChE J. 17 (1971) 115.

43. J.C. Melrose, AIChE J. 12 (1966) 986.

44. W. Rose, J. Appl. Phys. 29 (1958) 687.

45. N.L. Cross, R.G. Picknett, Trans. Faraday Soc. 59 (1963) 846.

46. A. Marmur, Langmuir 9 (1993) 1922.

47. G.I. Taylor, D.H. Michael, J. Fluid Mech. 58 (1973) 625.

48. M.L. Forcada, M.M. Jakas, A. Gras-Marti, J. Chem. Phys. 95 (1991) 706.

49. G. Debregeas, F. Brochard-Wyart, J. Colloid Interface Sci. 190 (1997) 134.

50. M.L. Fielden, R.A. Hayes, J. Ralston, Langmuir 12 (1996) 3721.

51. S. Ross, J. Phys. Colloid Chem. 54 (1950) 429.

52. P.R. Garrett, J. Colloid Interface Sci. 76 (1980) 587.

53. P.R. Garrett, in: P.R. Garrett (Ed.) Defoaming: Theory and Industrial Applications, M. Dekker, New York, 1993; Chapter 1.

54. R. Aveyard, P. Cooper, P.D.I. Fletcher, C.E. Rutherford, Langmuir 9 (1993) 604.

55. R. Aveyard, B.P. Binks, P.D.I. Fletcher, T.G. Peck, C.E. Rutherford, Adv. Colloid Interface Sci. 48 (1994) 93.

56. R. Aveyard, J.H. Clint, J. Chem. Soc. Faraday Trans. 93 (1997) 1397.

57. N.D. Denkov, P. Cooper, J.-Y. Martin, Langmuir 15 (1999) 8514.

58. N.D. Denkov, Langmuir 15 (1999) 8530.

59. D.H. Michael, Ann. Rev. Fluid Mech. 13 (1981) 189.

60. B.J. Lowry, P.H. Steen, Proc. R. Soc. London A, 449 (1995) 411.

61. J.N. Israelachvili, Intermolecular and Surface Forces, Academic Press, New York, 1992.

62. G. Mason, W.C. Clark, Brit. Chem. Engng. 10 (1965) 327.

63. M. Abramowitz, I.A. Stegun, Handbook of Mathematical Functions, Dover, New York, 1965.

64. E. Janke, F. Emde, F. Lösch, Tables of Higher Functions, McGraw-Hill, New York, 1960.

65. H.B. Dwight, Tables of Integrals and Other Mathematical Data, Macmillan Co., New York, 1961.

66. G.A. Korn, T.M. Korn, Mathematical Handbook, McGraw-Hill, New York, 1968.

67. A. Beer, Ann. d. Phys. u. Chem. 96 (1855) 1; ibid. p. 210.

68. W. Howe, Ph. D. Dissertation, Friedrich-Wilhelms Universität zu Berlin, 1887.

69. A.D. Myshkis, V.G. Babskii, N.D. Kopachevskii, L.A. Slobozhanin, A.D. Tyuptsov, Low-gravity Fluid Mechanics, Springer-Verlag, New York, 1987.

70. L.A. Slobozhanin, J.M. Perales, Phys. Fluids A 5 (1993) 1305.

71. J.C. Eriksson, S. Ljunggren, Langmuir 11 (1995) 2325.

72. T.L. Hill, An Introduction to Statistical Thermodynamics, Addison-Wesley, Reading, MA, 1962.

73. K.J. Mysels, Colloids Surf. 43 (1990) 241.

74. T.S. Horozov, C.D. Dushkin, K.D. Danov, L.N. Arnaudov, O.D. Velev, A. Mehreteab, G. Broze, Colloids Surf. A, 113 (1996) 117.

75. S.S. Dukhin, G. Kretzschmar, R. Miller, Dynamics of Adsorption at Liquid Interfaces, Elsevier, Amsterdam, 1995.

76. G.F.C. Searle, in: Experimental Physics, Cambridge Univ. Press, Cambridge, 1934; p.128.

77. J.F. Padday, A.R. Pitt, Phil. Trans. R. Soc. Lond. A 275 (1973) 489.

78. E.A. Boucher, M.J.B. Evans, Proc. R. Soc. Lond. A 346 (1975) 349.

79. T.I. Vogel, SIAM J. Appl. Math. 49 (1989) 1009.

80. J.W. Gibbs, The Scientific Papers of J.W. Gibbs, vol. 1, Dover, New York, 1961.

81. M. Volmer, Kinetik der Phasenbildung, Edwards Brothers, Ann Arbor, Michigan, 1945.

82. A.I. Rusanov, Phase Equilibria and Surface Phenomena, Khimia, Leningrad, 1967 (in Russian); Phasengleichgewichte und Grenzflächenerscheinungen, Akademie Verlag, Berlin, 1978.

83. V.P. Skripov, Metastable Liquid, Moscow, 1972 (in Russian).

84. F.F. Abraham, Homogeneous Nucleation Theory, Academic Press, New York, 1974.

85. E.D. Shchukin, A.V. Pertsov, E.A. Amelina, Colloid Chemistry, Moscow Univ. Press, Moscow, 1982 (in Russian).

86. A.W. Adamson, A.P. Gast, Physical Chemistry of Surfaces, 6th Edition, Wiley-Interscience, New York, 1997.

87. L.H. Cohan, J. Am. Chem. Soc. 60 (1938) 433.

88. J.C.P. Broekhoff, B.G. Linsen, in: B.G. Linsen (Ed.) Physical and Chemical Aspects of Adsorbents and Catalysts, Academic Press, New York, 1970; p. 1.

89. V.S. Yushchenko, V.V. Yaminsky, E.D. Shchukin, J. Colloid Interface Sci. 96 (1983) 307.

90. J.L. Parker, P.M. Claesson, P. Attard, J. Phys. Chem. 98 (1994) 8468.

91. R.S. Bradley, Q. Rev. (London) 5 (1951) 315.

92. P. Attard, Langmuir 16 (2000) 4455.